Full title

RNA polymerase mutations cause cephalosporin resistance in clinical *Neisseria gonorrhoeae* isolates

Authors

Samantha G. Palace[1,2], Yi Wang[1], Daniel H. F. Rubin[1], Michael A. Welsh[3], Tatum D. Mortimer[1], Kevin Cole[4], David W. Eyre[5], Suzanne Walker[3], Yonatan H. Grad[1,2,6]*

Affiliations

[1] Department of Immunology and Infectious Diseases, Harvard T. H. Chan School of Public Health, Boston, MA, USA

[2] Center for Communicable Disease Dynamics, Harvard T. H. Chan School of Public Health, Boston, MA, USA

[3] Department of Microbiology, Harvard Medical School, Boston, MA, USA

[4] Brighton and Sussex University Hospitals NHS Trust, Brighton, UK

[5] Big Data Institute, University of Oxford, Oxford, UK

[6] Division of Infectious Diseases, Brigham and Women's Hospital, Harvard Medical School, Boston, MA, USA

* To whom correspondence should be addressed: ygrad@hsph.harvard.edu

Abstract

Increasing *Neisseria gonorrhoeae* resistance to ceftriaxone, the last antibiotic recommended for empiric gonorrhea treatment, poses an urgent public health threat. However, the genetic basis of reduced susceptibility to ceftriaxone is not completely understood: while most ceftriaxone resistance in clinical isolates is caused by target site mutations in *penA*, others lack these mutations. Here, we show that *penA*-independent ceftriaxone resistance has evolved multiple times through distinct mutations in *rpoB* and *rpoD*. We identify five mutations in these genes that each increase resistance to ceftriaxone, including one mutation that arose independently in two lineages, and show that clinical isolates from multiple lineages are a single nucleotide change from ceftriaxone resistance. These RNA polymerase mutations result in large-scale transcriptional changes without altering susceptibility to other antibiotics, reducing growth rate, or deranging cell morphology. These results underscore the unexpected diversity of pathways to resistance and the importance of continued surveillance for novel resistance mutations.

Introduction

The rising incidence of *Neisseria gonorrhoeae* infection and antimicrobial resistance imperils effective therapy for gonococcal infections (Centers for Disease Control and Prevention, 2018; Demczuk et al., 2015; David W Eyre et al., 2018; Kirkcaldy et al., 2016). Current first-line therapy for gonorrhea relies on the extended spectrum cephalosporin ceftriaxone (CRO) as the backbone of treatment. Dual therapy with azithromycin was intended to delay the emergence of resistance, but rising azithromycin resistance rates have been reported (Kirkcaldy et al., 2016; Public Health England, 2018), resulting in revision of United Kingdom treatment guidelines to CRO monotherapy (Fifer, Saunders, Soni, Sadiq, & FitzGerald, 2019). With no clear next-line

agent, gonococcal resistance to ESCs is a problem of paramount clinical importance, illustrated by recent reports of treatment failure and global spread of a multidrug-resistant strain (David W Eyre et al., 2018; David W Eyre et al., 2019).

Rapid point-of-care diagnostics for antimicrobial susceptibility could help ensure efficacious treatment and improve stewardship (Crofts, Gasparrini, & Dantas, 2017; Tuite et al., 2017), with genotypic testing for known resistance determinants now implemented (Allan-Blitz et al., 2017; Fifer et al., 2019). In gonococcus, reduced susceptibility to ceftriaxone (CRO^{RS}) is most commonly associated with genetic variation in *penA* (PBP2), the primary target of ESCs (Kocaoglu & Carlson, 2015; Lindberg, Fredlund, Nicholas, & Unemo, 2007; David M. Whiley et al., 2010; S. Zhao et al., 2009). Because characterized *penA* alleles correlate very strongly with phenotypic CRO^{RS} in collections of clinical gonococcal isolates, the development of *penA*-targeted molecular diagnostic tests to rapidly evaluate gonococcal cephalosporin susceptibility is underway (Deng, Allan-Blitz, & Klausner, 2019; L. Zhao, Liu, Li, & Zhao, 2019).

However, these clinical collections often include isolates with ESC^{RS} that is not attributable to *penA* variation (Demczuk et al., 2015; Grad et al., 2016; Peng et al., 2019). For example, a recent report (Abrams et al., 2017) described the clinical gonococcal isolate GCGS1095, which has a cefixime (CFX) minimum inhibitory concentration (MIC) of 1 µg/mL and a CRO MIC of 0.5 µg/mL. These values are above the Center for Disease Control and Prevention's Gonococcal Isolate Surveillance Project (GISP) threshold values for CFX^{RS} (0.25µg/mL) and CRO^{RS} (0.125 µg/mL) (Kirkcaldy et al., 2016). The type II (non-mosaic) *penA* allele found in this isolate is not known to contribute to reduced cephalosporin susceptibility and is found in many ESC susceptible isolates (D. M. Whiley, Limnios, Ray, Sloots, & Tapsall, 2007). Loci distinct from *penA* can also contribute to ESC^{RS}. These include mutations in *porB*

that decrease drug permeability, mutations that enhance drug efflux by the MtrCDE pump, and non-mosaic mutations in penicillin-binding proteins (Lindberg et al., 2007; David M. Whiley et al., 2010). Mutations in *pilQ* have arisen during *in vitro* selection for cephalosporin resistance, although these variants have not been observed in clinical isolates (Johnson et al., 2014). Considering these other resistance-associated loci in addition to *penA* has been proposed as a way to refine sequence-based prediction of cephalosporin susceptibility (David W. Eyre et al., 2017). However, the genotype of GCGS1095 at these loci does not explain its high-level CRO^{RS} phenotype (Abrams et al., 2017). Rapid genotypic diagnostic tests for known resistance mutations would therefore misclassify this strain as CRO susceptible. Defining the basis for ESC^{RS} in this isolate and others like it is critical for the development of robust sequence-based diagnostics of antimicrobial susceptibility, for supporting public health genomic and phenotypic surveillance programs, and for understanding the biology underlying cephalosporin resistance.

Here, we employed an experimental transformation-based approach to identify the genetic basis of reduced susceptibility in three clinical isolates with high-level CRO^{RS}. We found that each of these isolates has unique mutations in the RNA polymerase holoenzyme (RNAP) that cause CRO^{RS}. One of these RNAP mutations is also present in a clinical isolate from the U.K., belonging to a genetically distinct clade, that has otherwise unexplained CRO^{RS}. We also identified an additional two RNAP mutations that arose *de novo* to cause CRO^{RS} *in vitro*. Furthermore, introducing RNAP mutations into diverse clinical isolates from multiple lineages was sufficient to cause high-level phenotypic CRO^{RS}, underscoring the ability of isolates from circulating clades to develop CRO^{RS} via a single mutation in RNA polymerase.

Results

A single missense mutation in *rpoB* is the genetic basis for reduced ceftriaxone susceptibility in the clinical isolate GCGS1095.

To identify the genetic basis of reduced susceptibility in GCGS1095, we transformed a ceftriaxone susceptible (CRO^S) recipient strain with genomic DNA from GCGS1095. We reasoned that minimizing the genetic distance between the resistant donor and susceptible recipient would improve the likelihood of identifying the causative region for CRO^{RS} and would reduce potentially confounding effects of divergent genomic backgrounds. Consequently, we selected GCGS0457, a close phylogenetic neighbor of GCGS1095 (Figure 1), as the CRO^S recipient for these experiments. Transformants were selected on CRO plates, and those that acquired the CRO^{RS} phenotype were characterized by whole genome sequencing to determine which variants they had inherited from GCGS1095.

We recovered multiple CRO^{RS} transformants. GCGS0457 did not develop spontaneous CRO^{RS} during culture or when transformed with autologous GCGS0457 genomic DNA. Whole genome sequencing of the CRO^{RS} transformants showed that each transformant inherited the same single nucleotide polymorphism (SNP) in *rpoB* (nucleotide change G602A), which encodes the RNA polymerase beta subunit RpoB (amino acid substitution R201H) (Figure 2). We named this allele *rpoB1*. These CRO^{RS} transformants did not acquire variants in genes known to contribute to reduced cephalosporin susceptibility, such as *penA*, *ponA*, *pilQ*, or *mtr* (David W. Eyre et al., 2017).

As RNA polymerase mutations have not been associated with cephalosporin resistance in *Neisseria*, we tested whether the *rpoB1* mutation is sufficient to confer CRO^{RS}. To do so, we performed directed transformation of GCGS0457 with a ~1.5 kilobase PCR product surrounding the variant position of *rpoB1*. With the exception of the single *rpoB* G602A nucleotide change,

the sequence of this PCR product was identical to the parental GCGS0457 sequence. Transformation with the *rpoB1* allele amplified from GCGS1095 yielded multiple CRO^{RS} transformants, whereas transformation with control PCR products amplified from a strain containing wild-type *rpoB* yielded none. Sanger sequencing confirmed the presence of the expected SNP in each resistant transformant. Representative CRO^{RS} transformants were further examined by whole genome sequencing, which ruled out spontaneous mutations. The CRO MIC of the *rpoB1* transformant strain GCGS0457 RpoB^{R201H} was 0.25 μg/mL, a more than ten-fold increase from recipient strain GCGS0457 (CRO MIC 0.016 μg/mL) (Table 1). This transformant MIC is similar to the MIC of the parental CRO^{RS} isolate GCGS1095 (Table 1), indicating that introduction of this SNP is sufficient to fully recapitulate the CRO^{RS} phenotype in the GCGS0457 background.

RNA polymerase mutations explain CRO^{RS} in other clinical isolates.

GCGS1014 is a phylogenetic neighbor of GCGS1095 that also has unexplained CRO^{RS} (Figure 1; Table 1). The close phylogenetic relationship between these isolates led us to hypothesize that they would share the same mechanism of CRO^{RS}. However, the GCGS1014 isolate lacks the *rpoB1* allele identified in GCGS1095. In fact, among the 1102 sequenced isolates in the GISP collection, the *rpoB1* allele is unique to GCGS1095 (Supplemental file 1).

To define the genetic basis of CRO^{RS} in GCGS1014, we used the same unbiased transformation approach as described above, again using the CRO^{S} neighbor GCGS0457 as the recipient strain. The CRO^{RS} transformants from GCGS1014 gDNA did not have mutations in *rpoB* or in other characterized resistance-associated genes. Instead, all CRO^{RS} transformants inherited a single nucleotide substitution in *rpoD* (nucleotide G292A), which encodes the major

housekeeping sigma factor RpoD, or σ^{70} (amino acid substitution E98K) (Figure 2). This allele, *rpoD1*, is present in the CRO^{RS} donor GCGS1014 but not in GCGS1095 (Table 1) or in any other isolate from the GISP collection (Supplemental file 1). To test the ability of the *rpoD1* allele to confer CRO^{RS} to a susceptible strain, we transformed GCGS0457 with a ~1.5 kilobase PCR product that includes the single variant position in *rpoD1*. As with the directed transformation of *rpoB1*, the *rpoD1* allele amplified from GCGS1014 transformed GCGS0457 to high-level CRO^{RS}, but control PCR products amplified from strains with wild-type *rpoD* did not. The presence of the *rpoD1* allele in resistant transformants was confirmed by Sanger sequencing and by whole genome sequencing, which also ruled out the possibility of spontaneous mutations causing the CRO^{RS} phenotype. The *rpoD1* transformant strain GCGS0457 RpoD^{E98K} had a CRO MIC of 0.125 μg/mL, similar to that of the parental CRO^{RS} isolate GCGS1014 (Table 1).

As the CRO^{RS} phenotype in GCGS1095 and GCGS1014 is caused by distinct RNAP mutations, we examined alleles of RNAP components in each of the 1102 genomes in the GISP collection (Grad et al., 2016) to identify additional RNAP variants that might explain other cases of uncharacterized CRO^{RS} (Supplementary file 1). We found that the isolate GCGS1013 has a 12-basepair in-frame internal deletion in *rpoD*, resulting in the deletion of amino acids 92-95 (Figure 2); GCGS1013 has a CRO^{RS} phenotype but does not have a CRO^{RS}-associated *penA* allele (CRO MIC 0.125 μg/mL; Table 1). Transformation of this allele, *rpoD2*, into the susceptible recipient GCGS0457 increased CRO resistance to 0.125 μg/mL (Table 1). The *rpoD2* allele is also present in a clinical gonococcal isolate from a recent United Kingdom strain collection (De Silva et al., 2016). This isolate, GCPH44 (genome accession number SRR3360905), has a CRO^{RS} phenotype (CRO MIC 0.125 μg/mL) and represents a distinct phylogenetic lineage from that of GCGS1013 (Figure 1). Like GCGS1013, the CRO^{RS}

phenotype of GCPH44 is not attributable to variation in *penA* or other known resistance determinants (Table 1).

The amino acids deleted in the *rpoD2* allele (Δ92-95) are in a similar region of the RpoD protein as the single amino acid change in the *rpoD1* allele (E98K) (Figure 2A). This flexible portion of the σ^{70} 1.1 domain is not included in published RNA polymerase holoenzyme crystal structures. Modeling of *E. coli* RNAP predicts that σ^{70} 1.1 interacts with the DNA channel formed by the β subunit encoded by *rpoB* prior to open complex formation (Murakami, 2013). In *E. coli*, the RpoB residue homologous to the substituted amino acid in *rpoB1* (*E. coli* RpoB R197) is located on the surface of the β lobe structure that makes up this same channel (Figure 2B). Taken together, these results demonstrate that RNAP-mediated CRO^{RS} has arisen multiple times in clinical isolates of *N. gonorrhoeae*, and that these different mutations affect a similar region of the RNAP holoenzyme. They may therefore act via a similar mechanism to effect phenotypic CRO^{RS}.

Clinical isolates from multiple lineages can achieve high-level CRO^{RS} via a single nucleotide change in *rpoB*.

The *rpoB1* and *rpoD1* alleles each differ from wild-type by a single nucleotide. The ability of these mutations to cause high-level CRO^{RS} when introduced into the susceptible strain GCGS0457 indicates that some gonococcal isolates are a single-step mutation from CRO^{RS}. Because three of the four clinical isolates we identified with RNAP-mediated CRO^{RS} are clustered in one part of the gonococcal phylogeny (Figure 1), we tested whether acquisition of CRO^{RS} via this pathway is limited to strains within this particular clade – which would suggest

that one or more genetic background factors are required – or whether RNAP mutation represents a broadly accessible evolutionary trajectory to CRO^{RS}.

To address this question, we sought to transform genetically diverse recipient strains to CRO^{RS} with the *rpoB1* allele. In a panel of 17 clinical isolates from the GISP collection, we found five additional recipients dispersed throughout the phylogeny that acquired phenotypic CRO^{RS} following directed transformation with *rpoB1* (Figure 1; Supplementary file 1). The remaining 12 isolates, as well as the laboratory strain 28BL, did not readily produce CRO^{RS} *rpoB1* transformants after 1-2 transformation attempts. These results indicate that genetic background compatibility with this resistance mechanism is not limited to a single gonococcal lineage or to recipients with particular alleles of any RNA polymerase component (Supplementary file 1).

A clinical isolate develops high-level CRO^{RS} *in vitro* through spontaneous *rpoB* mutations.

While screening isolates for genetic compatibility with *rpoB*-mediated CRO^{RS} in the directed transformation experiments described above, we tested isolates in parallel for spontaneous development of CRO^{RS}. We found that the CRO^{S} isolate GCGS0364, located in a similar part of the phylogeny as the resistant isolates GCGS1095, GCGS1014, and GCGS1013 (Figure 1), produced stably CRO^{RS} derivatives when selected on CRO *in vitro*. Sanger sequencing of the *rpoB* locus in two of these derivatives identified two different spontaneous *rpoB* mutations: *rpoB2* (nucleotide change C470T, amino acid change P157L) and *rpoB3* (nucleotide change G473T, amino acid change G158V) (Figure 2A). These *de novo* RpoB mutations are predicted to occur in the same β-sheet as the *rpoB1* variant position (R201H) identified in GCGS1095 (Figure 2B). Directed transformation of *rpoB2* or *rpoB3* into the

184 parental (CRO^{S}) GCGS0364 isolate conferred phenotypic CRO^{RS}, increasing the CRO MIC
185 more than 20-fold from 0.023 μg/mL to 0.5-0.75 μg/mL (Table 1).
186
187 **RNAP-mediated CRO^{RS} acts via a cephalosporin-specific mechanism.**
188 As optimal function of RNA polymerase machinery is required for bacterial fitness, we
189 tested the hypothesis that these RNAP mutations are not specific cephalosporin resistance
190 mutations but instead cause a slow-growth or general stress response phenotype that
191 nonspecifically increases resistance to diverse classes of antimicrobial compounds.
192 As expected, the *rpoB1*, *rpoD1*, or *rpoD2* alleles conferred reduced susceptibility to
193 cefixime (another third-generation cephalosporin) when transformed into the CRO^{S} recipient
194 GCGS0457. However, these alleles did not affect susceptibility to antimicrobial drugs that do not
195 target the cell wall, including ciprofloxacin, tetracycline, azithromycin, and rifampicin.
196 Surprisingly, these mutations also failed to confer resistance to the non-cephalosporin β-lactams
197 penicillin and ertapenem. The apparent cephalosporin specificity of these RNAP mutations in the
198 GCGS0457 background is consistent with in the antibiotic susceptibility profiles of the three
199 clinical isolates from which they were identified (GCGS1095 for *rpoB1*, GCGS1014 for *rpoD1*,
200 and GCGS1013 for *rpoD2*) (Table 2).
201 GCGS0457 *rpoB1* and GCGS0457 *rpoD1* transformants were further examined for
202 evidence of a slow growth phenotype that might increase antibiotic tolerance. When grown on
203 GCB agar (Difco), neither of these transformants had a reduced growth rate compared to the
204 parental GCGS0457 strain (Figure 3A). Furthermore, the *rpoB1* and *rpoD1* transformants had no
205 gross defects in cell morphology by transmission electron microscopy (TEM) (Figure 3B),
206 although transformants were slightly smaller than the parental GCGS0457 strain (Supplementary

Figure 1). Taken together, these results do not support the hypothesis that RNAP mutations reduce CRO susceptibility via a slow growth or nonspecific tolerance phenotype.

CRO^{RS}-associated RNAP mutations induce widespread transcriptional changes.

To measure the functional effect of the *rpoB1* and *rpoD1* alleles on RNA polymerase, we characterized the transcriptional profiles of the CRO^{RS} isolates GCGS1095 (*rpoB1*) and GCGS1014 (*rpoD1*) and the susceptible isolate GCGS0457 by RNA-seq. The transcriptional profiles of the CRO^{RS} isolates were similar to one another but distinct from GCGS0457 (Supplementary Figure 2), with 1337 and 1410 annotated ORFs significantly altered in abundance, respectively. The transcriptomic differences we observe may partly reflect the genetic distance between these isolates (C. B. Wadsworth, Sater, Bhattacharyya, & Grad, 2019), as the resistant strains GCGS1095 and GCGS1014 are more closely related to one another than they are to GCGS0457. We therefore compared GCGS0457 to its isogenic CRO^{RS} transformants GCGS0457 RpoB^{R201H} and GCGS0457 RpoD^{E98K}. The *rpoB1* and *rpoD1* alleles each profoundly altered the transcriptional profile of GCGS0457: 1278 annotated ORFs in GCGS0457 RpoD^{E98K} and 1218 annotated ORFs in the GCGS0457 RpoB^{R201H} were differentially expressed relative to the parental GCGS0457 strain. The transcriptional profiles of the two transformants were very similar to one another (Supplementary Figure 2), indicating that these different mutations have similar functional consequences. Overall, a total of 890 annotated ORFs were differentially expressed in all four CRO^{RS} strains (the two CRO^{RS} isolates and two transformants in the GCGS0457 background) compared to GCGS0457. The vast majority of the transcriptional changes are small in magnitude: 805/890 (90%) are less than 2-fold differentially expressed in one or more of the CRO^{RS} strains.

Altered expression of resistance-associated genes such as efflux pumps and β-lactamases is a common mechanism of transcriptionally-mediated drug resistance. Although these strains lack a TEM-1 β-lactamase (Grad et al., 2016), increased expression of the gonococcal MtrCDE efflux pump is known to increase resistance to β-lactams, including cephalosporins (Lindberg et al., 2007). However, transcription of the operon encoding this pump is not elevated in the CRO^{RS} RNAP mutants (Supplementary Figure 3), nor is it differentially upregulated in response to drug exposure in these strains (Supplementary Figure 4).

In vitro evolution studies that evolve cephalosporin resistance in *N. gonorrhoeae* identified inactivating mutations in the type IV pilus pore subunit PilQ (Johnson et al., 2014; S. Zhao, Tobiason, Hu, Seifert, & Nicholas, 2005), although similar *pilQ* mutations have not been identified in clinical isolates, presumably because colonization requires pilus-mediated adhesion to epithelial cells (Kellogg, Peacock, Deacon, Brown, & Pirkle, 1963; Rudel, van Putten, Gibbs, Haas, & Meyer, 1992). Notably, *pilQ* transcription is reduced in the GCGS0457 *rpoB1* and GCGS0457 *rpoD1* transformants, as well as in the CRO^{RS} isolates GCGS1095 and GCGS1014 (Supplementary Figure 3 and 4). The effect of hypomorphic *pilQ* expression on cephalosporin susceptibility has not been described, but it is possible that reducing *pilQ* transcript levels may confer the benefits of inactivating *pilQ* mutations without eliminating pilus-mediated attachment and colonization altogether.

CRO^{RS}-associated RNAP mutations alter the abundance of cell wall biosynthesis enzymes.

Since ESCs, like other β-lactams, block cell wall biosynthesis by covalently inhibiting penicillin-binding proteins (PBPs), we examined how CRO^{RS}-associated RNAP mutations affect expression of enzymes in this target pathway. *N. gonorrhoeae* encodes four known PBPs

(Obergfell, Schaub, Priniski, Dillard, & Seifert, 2018; Sauvage, Kerff, Terrak, Ayala, & Charlier, 2008): the essential high-molecular weight bifunctional transpeptidase/transglycosylase PBP1 (encoded by *ponA*); the essential high-molecular weight transpeptidase PBP2 (encoded by *penA*), which is the primary target of ESCs (Kocaoglu & Carlson, 2015; S. Zhao et al., 2009); and the nonessential carboxypeptidases PBP3 (encoded by *dacB*) and PBP4 (encoded by *pbpG*). In addition to these canonical PBPs, *N. gonorrhoeae* genomes include DacC (encoded by *dacC*), a third putative low-molecular weight carboxypeptidase that lacks conserved active site motifs (Obergfell et al., 2018). A homologue of the L,D-transpeptidase YnhG is also present in the genome, although it has not been reported to be functional in *N. gonorrhoeae*.

Increased expression of drug targets can lead to decreased drug susceptibility, but CRO^{RS}-associated RNAP mutations did not increase mRNA or protein abundance of the CRO target PBP2 (Figure 4). Transcription of the putative L,D-transpeptidase gene *ynhG* is also unchanged in the CRO^{RS} strains (Supplementary Figure 3). By contrast, PBP1 (*ponA*) is upregulated in each of the CRO^{RS} strains compared to GCGS0457, while expression of PBP3, *pbpG*, and *dacC* is decreased in these strains (Figure 4A-B). Similar expression patterns were observed in the presence of sub-inhibitory CRO (Supplementary Figure 4).

These altered PBP expression patterns are reflected in the cell wall structure of the CRO^{RS} strains: reduced expression of the carboxypeptidases results in more peptidoglycan with pentapeptide stems (Figure 5 and Supplementary Table 2), in agreement with reported structural changes of cell walls from strains lacking the DacB carboxypeptidase (Obergfell et al., 2018). The increased expression of PBP1 in these RNAP mutants does not appear to increase the abundance of crosslinked peptidoglycan (Supplementary Figure 5 and Supplementary Table 2).

Discussion

We have identified five different CRO^{RS}-associated RNA polymerase alleles. Three of these – *rpoB1*, *rpoD1*, and *rpoD2* – are the genetic basis of high-level reduced ESC susceptibility in clinical isolates with previously unexplained resistance phenotypes. The remaining two arose spontaneously during culture, indicating that the RNAP alleles described in this work are likely only a subset of functionally similar mutations that could arise in clinical isolates. Clinical isolates from diverse genetic backgrounds can achieve high-level CRO^{RS} via these RNAP mutations. This is highlighted by the appearance of the *rpoD2* allele in a second clinical isolate belonging to a genetically distinct clade. Because this isolate is a member of a large clade that includes many closely related isolates, this result illustrates the concerning potential of these mutations to cause *penA*-independent CRO^{RS} in globally distributed strains and the importance of including these mutations in ongoing surveillance efforts.

Among the isolates of the GISP collection, there was no evidence for sustained transmission of the CRO^{RS} RNAP mutant isolates (Figure 1), perhaps indicating that fitness costs associated with these RNAP variants have prevented their spread. However, it is important to note that the CRO^{RS} isolates GCGS1095, GCGS1014, and GCGS1013 are susceptible to azithromycin (Table 2). This susceptibility may be an alternative explanation for the failure of these RNAP mutations to spread in an era of azithromycin/ceftriaxone combination therapy.

RNA polymerase mutations have been identified as mediators of diverse phenotypes, such as reduced susceptibility to phage lysis (Atkinson & Gottesman, 1992; Obuchowski et al., 1997) and antimicrobial drugs, including cell wall biosynthesis inhibitors (Cui et al., 2010; Kristich & Little, 2012; Y. H. Lee, Nam, & Helmann, 2013; Penwell et al., 2015; Wang et al., 2017). These mutations often arise during *in vitro* evolution experiments, and are typically

299 described as artifacts of *in vitro* conditions, as the presumed pleiotropy of such mutations is
300 typically thought to be prohibitively deleterious. This description of resistance-associated RNAP
301 mutations in isolates collected from symptomatic patients demonstrates that, at least in the case
302 of CRO^{RS} in *N. gonorrhoeae*, clinical isolates can acquire resistance via RNAP mutation while
303 still maintaining sufficient fitness to cause disease. Similar results have been reported regarding
304 the role of *rpoB* mutation in decreased susceptibility to vancomycin in staphylococcal species
305 (Guérillot et al., 2018; J. Y. H. Lee et al., 2018; Watanabe, Cui, Katayama, Kozue, & Hiramatsu,
306 2011).

307 In accordance with this model, the RNAP mutations identified in these CRO^{RS} isolates
308 result in an apparently narrowly-targeted phenotypic change: RNAP mutants acquire resistance
309 to cephalosporins but not other classes of antimicrobial drugs, show no growth defect *in vitro*,
310 and display broad but small-magnitude changes to transcript levels, indicating that RNAP
311 mutation may be a valid approach to fine-tuning bacterial physiology for enhanced survival
312 under certain adverse conditions, such as antibiotic exposure.

313 The observation that the RNAP mutations identified here neither decrease susceptibility
314 to other antimicrobials nor alter growth phenotypes supports the hypothesis that these mutations
315 generate a “fine-tuning” cephalosporin-specific resistance mechanism, as opposed to a large-
316 scale physiological shift toward a generally antibiotic-tolerant state. Altered activity of the RNA
317 polymerase transcription machinery likely results in this type of drug-specific reduced
318 susceptibility. RNAP variants differentially express multiple transcripts relating to the
319 cephalosporin mode of action. For example, while PBP2 levels are unaffected, the increase of
320 PBP1 expression may contribute to cephalosporin resistance. PBP1 and PBP2 both catalyze
321 transpeptidation, but PBP1 is not efficiently inhibited by third-generation cephalosporins

(Kocaoglu & Carlson, 2015), suggesting that increased PBP1 levels may partly compensate for CRO-inhibited PBP2 during drug treatment. The RNAP variants simultaneously reduce D,D-carboxypeptidase expression, increasing the pool of pentapeptide peptidoglycan monomers available for transpeptidation by PBP1 and PBP2. Decreased expression of pilus pore components in these mutants may also contribute to CRO^{RS} by reducing permeability of the outer membrane to cephalosporins (Chen et al., 2004; Johnson et al., 2014; Nandi, Swanson, Tomberg, & Nicholas, 2015; S. Zhao et al.). These expression changes and others may work additively or synergistically to increase drug resistance. The pleiotropy of RNAP mutations may thus enable a multicomponent resistance mechanism to emerge following a single genetic change.

This result has important implications regarding the biology underlying cephalosporin resistance, the potential for *de novo* evolution of resistance under cephalosporin monotherapy, and the accuracy of sequence-based diagnostics. The identification of five independent mutations in two separate components of the RNA polymerase machinery illustrates challenges faced by computational genomics strategies to define new resistance alleles, especially because there are other variants in these genes – such as rifampicin resistance mutations in *rpoB* – that do not confer CRO^{RS}. Continued isolate collection, phenotypic characterization, and traditional genetic techniques will be critical for defining emerging resistance mechanisms (Hicks, Kissler, Lipsitch, & Grad, 2019). The observation that multiple lineages can gain CRO resistance through RNAP mutations further underscores the need to monitor for the development of CRO^{RS} through pathways other than *penA* mutation, particularly as the ESCs are increasingly relied upon for treatment. Identifying these alternative genetic mechanisms of reduced susceptibility is needed to

support the development of accurate and reliable sequence-based diagnostics that predict CRO susceptibility, as well as to aid in the design of novel therapeutics.

Methods

Bacterial strains and culture conditions. Strains are presented in Supplementary Table 1. Except where otherwise specified, *N. gonorrhoeae* was cultured on GCB agar (Difco) with Kellogg's supplements (GCB-K) (Kellogg et al., 1963) at 37°C in a 5% CO_2 atmosphere. Antibiotic susceptibility testing of *N. gonorrhoeae* strains was performed on GCB media supplemented with 1% IsoVitaleX (Becton Dickinson) via agar dilution or Etest (bioMérieux). *E. coli* strains were cultured in LB medium at 37°C. Media were supplemented as appropriate with chloramphenicol (20 μg/mL for *E. coli*; 1 μg/mL for *N. gonorrhoeae*).

Transformation of reduced cephalosporin susceptibility with genomic DNA. The CRO^S recipient strain GCGS0457 was transformed with genomic DNA from GCGS1014 and GCGS1095. Transformations were conducted in liquid culture as described (Morse, Johnson, Biddle, & Roberts, 1986; Crista B Wadsworth, Arnold, Abdul Sater, & Grad, 2018). Briefly, piliated *N. gonorrhoeae* was suspended in GCP medium (15 g/L protease peptone 3, 1 g/L soluble starch, 4 g/L dibasic K_2HPO_4, 1 g/L monobasic KH_2PO_4, 5 g/L NaCl) with Kellogg's supplement, 10mM $MgCl_2$, and approximately 100 ng genomic DNA. Suspensions were incubated for 10 minutes at 37°C with 5% CO_2. Transformants were allowed to recover on nonselective agar for 4-5 hours. After recovery, transformants were plated on GCB-K ceftriaxone gradient agar plates, which were prepared by allowing a 40 μL droplet of 5 μg/mL ceftriaxone to dry onto a GCB-K agar plate. Transformations performed with GCGS0457 genomic DNA served as controls to monitor for spontaneous CRO^{RS} mutation. After outgrowth

367 at 37°C in 5% CO_2, colonies growing within the ceftriaxone zone of inhibition were subcultured
368 for further analysis.
369 **Transformation of RNA polymerase mutations.** ~1.5kb PCR fragments surrounding the *rpoB*
370 and *rpoD* loci of interest were amplified using the primer pairs RpoB-US (5'-
371 ATGCCGTCTGAATATCAGATTGATGCGTACCGTT-3') and RpoB-DS (5'-
372 CGTACTCGACGGTTGCCCAAG-3') or RpoD-US (5'-AACTGCTCGGACAGGAAGCG-3')
373 and RpoD-DS (5'-CGCGTTCGAGTTTGCGGATGTT-3'). The 12-bp DNA uptake sequence
374 (DUS) for *N. gonorrhoeae* (Ambur, Frye, & Tønjum, 2007) was added to the 5' end of the
375 RpoB-US primer (underlined) to enhance transformation efficiency with the PCR product; a
376 DUS was not added to the RpoD-US or RpoD-DS primers, as the PCR product amplified by
377 these primers includes two endogenous DUS regions. CRO^S recipient strains were transformed
378 with 200-300 ng purified PCR products and transformants were selected for CRO^{RS} as above.
379 Transformation reactions performed with wildtype alleles (*rpoB*$^+$ from GCGS1014; *rpoD*$^+$ from
380 GCGS1095) served as controls to monitor for spontaneous CRO^{RS} mutation.
381 **Sequencing and analysis.** Following undirected transformation of GCGS0457 with GCGS1014
382 or GCGS1095 genomic DNA, or directed transformation of GCGS0457 with PCR products,
383 CRO^{RS} transformants were analyzed by whole genome sequencing. Genomic DNA of
384 transformants was purified with the PureLink Genomic DNA Mini kit (Life Technologies) and
385 sequencing libraries were prepared as described (Kim et al., 2017). Paired-end sequencing of
386 these libraries was performed on an Illumina MiniSeq (Illumina). Reads were aligned to the *de*
387 *novo* assembly of the GCGS0457 genome (European Nucleotide Archive, accession number
388 ERR855051) using bwa v0.7.8 (Li & Durbin, 2010), and variant calling was performed with
389 pilon v1.22 (Walker et al., 2014).

Whole genome assembly and annotation. Whole genome sequencing reads from the GISP collection were assembled using Velvet (Zerbino & Birney, 2008) as previously described (Grad 2016). Spades v 3.12 (Bankevich et al., 2012) was used for *de novo* assembly of GCPH44. Contigs were corrected by mapping reads back to the assembly (--careful), and contigs with less than 10X coverage or fewer than 500 nucleotides were removed. Reads were also mapped to the reference genome NCCP11945 (NC_011035.1) with bwa mem v0.7.15 (Li, 2013). Variants were identified with Pilon v 1.16 (Walker et al., 2014) using a minimum depth of 10 and minimum mapping quality of 20. SNPs, small deletions, and uncertain positions were incorporated into the reference genome to create pseudogenomes. For each isolate in the GISP collection and in the United Kingdom collection (De Silva et al., 2016), the sequence of RNA polymerase components was identified using BLASTn (ncbi-blast v2.2.30) (Supplemental File 1).

Phylogenetic analysis. Recombinant regions of the pseudogenome alignment were detected by Gubbins (Croucher et al., 2015), and the maximum likelihood phylogenetic tree was estimated from this masked alignment using RAxML (Stamatakis, 2014). The phylogeny was visualized using ITOL (Letunic & Bork, 2019).

Growth curves. Bacterial cells grown overnight on GCB-K plates were suspended in tryptic soy broth to OD_{600} 0.01. Three replicate GCB-K plates per time point were inoculated with 0.1 mL of this suspension and incubated at 37°C with 5% CO_2. At each time point, the lawn of bacterial growth from each of three replicate plates was suspended in tryptic soy broth. Serial dilutions were plated on GCB-K to determine total CFUs per plate. CFU counts were normalized to the initial inoculum density (CFUs measured at time 0) for each replicate.

Transmission electron microscopy. Bacterial cells grown overnight on GCB-K plates were suspended in liquid GCP medium with 1% Kellogg's supplement and 0.042% $NaHCO_3$ to OD_{600}

0.1. Suspensions were incubated at 37°C with aeration for 2 hours to allow cultures to return to log phase. Cell pellets were collected by centrifugation and fixed for at least two hours at room temperature in 0.2M cacodylate buffer with 2.5% paraformaldehyde, 5% glutaraldehyde, and 0.06% picric acid. Fixed pellets were washed in 0.1M cacodylate buffer and postfixed with 1% Osmiumtetroxide (OsO_4)/1.5% Potassiumferrocyanide (KFeCN6) for 1 hour, washed 2x in water, 1x Maleate buffer (MB) 1x and incubated in 1% uranyl acetate in MB for 1hr followed by 2 washes in water and subsequent dehydration in grades of alcohol (10min each; 50%, 70%, 90%, 2x10min 100%). The samples were then put in propyleneoxide for 1 hr and infiltrated ON in a 1:1 mixture of propyleneoxide and TAAB Epon (Marivac Canada Inc. St. Laurent, Canada). The following day the samples were embedded in TAAB Epon and polymerized at 60 degrees C for 48 hrs. Ultrathin sections (~60nm) were cut on a Reichert Ultracut-S microtome, picked up on to copper grids stained with lead citrate and examined in a JEOL 1200EX Transmission electron microscope or a TecnaiG² Spirit BioTWIN and images were recorded with an AMT 2k CCD camera.

Transcriptomics. RNA isolation and sequencing was performed from *N. gonorrhoeae* strains as described (Crista B Wadsworth et al., 2018). Bacterial cells grown on GCB-K plates for 17 hours were suspended in liquid GCP medium with 1% IsoVitaleX and 0.042% $NaHCO_3$ to OD_{600} 0.1. Suspensions were incubated at 37°C with aeration for 2-3 hours to allow cultures to return to log phase. Cells were collected to measure baseline transcriptional profiles. For samples measuring the effect of drug exposure, 0.008 µg/mL CRO was added and cultures were incubated at 37°C for an additional 90 minutes before cell collection. RNA was purified with the Direct-Zol kit (Zymo). Transcriptome libraries were prepared at the Broad Institute at the Microbial 'Omics Core using a modified version of the RNAtag-seq protocol (Rudy et al., 2015). Five hundred

436 nanograms of total RNA was fragmented, depleted of genomic DNA, dephosphorylated, and
437 ligated to DNA adapters carrying 5'-AN8-3' barcodes of known sequence with a 5' phosphate
438 and a 3' blocking group. Barcoded RNAs were pooled and depleted of rRNA using the RiboZero
439 rRNA depletion kit (Epicentre). Pools of barcoded RNAs were converted to Illumina cDNA
440 libraries in two steps: (i) reverse transcription of the RNA using a primer designed to the
441 constant region of the barcoded adapter with addition of an adapter to the 3' end of the cDNA by
442 template switching using SMARTScribe (Clontech) as described previously (Zhu, Machleder,
443 Chenchik, Li, & Siebert, 2001); (ii) PCR amplification using primers whose 5' ends target the
444 constant regions of the 3' or 5' adapter and whose 3' ends contain the full Illumina P5 or P7
445 sequences. cDNA libraries were sequenced on the Illumina Nextseq 500 platform to generate 50-
446 bp paired-end reads. Barcode sequences were removed, and reads were aligned to the FA1090
447 reference genome. Differential expression analysis was conducted in DESeq2 v.1.16.1 (Love,
448 Huber, & Anders, 2014).
449 **Sequence data availability.** Genomic and transcriptomic read libraries are available from the
450 NCBI SRA database (accession number PRJNA540288).
451 **PBP abundance measurement.** Protein abundance of PBP1, PBP2, and PBP3 was calculated
452 using the fluorescent penicillin derivative bocillin-FL (Thermo Fisher). *N. gonorrhoeae* strains
453 from overnight cultures were suspended in liquid GCP medium supplemented with 1%
454 IsoVitalex and 0.042% $NaHCO_3$ to a density of OD_{600} 0.1. Suspensions were incubated with
455 aeration at 37°C for 2.5-3 hours. Bacterial cells were collected by centrifugation, washed once
456 with 1 mL of sterile phosphate-buffered saline (PBS), and resuspended in PBS 5 μg/mL bocillin-
457 FL and 0.1% dimethyl sulfoxide (DMSO) to a final concentration of 1 mL of OD_{600} 0.5 per 50
458 μL suspension. Bocillin-FL suspensions were incubated for 5 minutes. An equal volume 2x

459 SDS-PAGE sample buffer (Novex) was added and samples were boiled for 5 minutes. Proteins
460 in 30 µL of each suspension were separated by SDS-PAGE on 4-12% Tris-Glycine protein gels
461 (Novex), which were visualized on a Typhoon imager (Amersham) (excitation 488 nm/emission
462 526 nm) to detect bocillin-FL fluorescence. Densitometry was performed with ImageJ
463 (Schneider, Rasband, & Eliceiri, 2012). Total bocillin-FL fluorescent signal was calculated for
464 each sample, and the proportional contribution of individual PBPs to this signal was reported.
465 **Muropeptide analysis.** *N. gonorrhoeae* strains were cultured for approximately 18 hours at
466 37°C with agitation in GCP medium supplemented with Kellogg's reagent and 0.042% $NaHCO_3$.
467 Peptidoglycan was isolated and digested as described (Kühner, Stahl, Demircioglu, & Bertsche,
468 2014) with minor modifications. Briefly, bacterial cells were pelleted by centrifugation,
469 suspended in 1 mL 1M NaCl, and incubated at 100°C for 20 minutes. Samples were centrifuged
470 for one minute at 18,000×*g*. Pellets were washed three times with water, suspended in 1 mL
471 water, and placed in a bath sonicator for 30 minutes. 0.5 mL 0.1M Tris pH 6.8, 40 µg/mL RNase,
472 and 16 µg/mL DNase were added to each sample; samples were incubated with shaking at 37°C
473 for two hours, with the addition of 16 µg/mL trypsin after the first hour of incubation. Samples
474 were heated to 100°C for 5 minutes to inactivate enzymes, then centrifuged for 3 minutes at
475 18,000×*g* to pellet peptidoglycan. Pellets were washed with 1 mL aliquots of water until the
476 suspension pH measured between 5 and 5.5. Peptidoglycan was then resuspended in 0.2 mL
477 12.5mM NaH_2PO_4 pH 5.5 with 500 U/mL mutanolysin and incubated with shaking at 37°C for
478 16 hours. Samples were heated to 100°C for 5 minutes to inactivate mutanolysin and centrifuged
479 for 5 minutes at 18,000×*g* to pellet debris. The supernatant, containing solubilized muropeptides,
480 was removed to new tubes, and 50 µL 10mg/mL $NaBH_4$ was added to each. Samples were

481 incubated at room temperature for 30 minutes and then the pH was adjusted to 2-3 with 85%
482 H_3PO_4.

483 LC-MS was conducted using an Agilent Technologies 1200 series HPLC in line with an
484 Agilent 6520 Q-TOF mass spectrometer operating with electrospray ionization (ESI) and in
485 positive ion mode. The muropeptide fragments were separated on a Waters Symmetry Shield
486 RP18 column (5 µm, 4.6 x 250 mm) using the following method: 0.5 mL/minute solvent A
487 (water, 0.1% formic acid) for 10 minutes followed by a linear gradient of 0% solvent B
488 (acetonitrile, 0.1% formic acid) to 20% B over 90 minutes.

489

490 **Acknowledgements.**

491 We thank the Centers for Disease Control and Prevention Gonococcal Isolate
492 Surveillance Project, Joseph Dillard, Steven Johnson, and Caroline Genco for generously
493 providing strains; Georgia Lagoudas and Paul Blainey for sequencing undirected transformants;
494 Jessica Alexander, Jonathan Livny, and the Broad Institute Microbial 'Omics Core for RNAseq
495 support; the Harvard Medical School Electron Microscopy Facility for TEM imaging; and Crista
496 Wadsworth and Mohamad Rustom Abdul Sater for advising on analysis pipelines.

497 This work was supported by the Richard and Susan Smith Family Foundation (to YHG)
498 and the National Institutes of Health R01 AI132606 (to YHG), R01 GM76710 (to SW), and F32
499 GM123579 (to MAW).

500

501 **Author contributions.** SGP and YHG designed and coordinated the study. SGP, YW, DHFR,
502 MAW, TDM, and KC performed experiments and data analysis. SGP and YHG wrote the

503 manuscript with input from all authors. MAW and SW provided critical manuscript revision.

504 SW, DWE, and YHG contributed funding, resources, and supervision.

Table 1. Selected strains, phenotypic ceftriaxone susceptibility, and relevant genotypes.

strain	CRO MIC (μg/mL)	*penA* (PBP2)	*ponA* (PBP1)	PorB 120/121	RpoB	RpoD
GCGS0457	0.016	Type II non-mosaic (NG STAR 2.002)	421P	120G/121V	wildtype	wildtype
GCGS1095	0.5	Type II non-mosaic (NG STAR 2.002)	421P	120N/121A	R201H (*rpoB1*)	wildtype
GCGS1014	0.125	Type II non-mosaic (NG STAR 2.002)	421P	120D/121A	wildtype	E98K (*rpoD1*)
GCGS1013	0.125	Type II non-mosaic (NG STAR 2.002)	421P	120G/121A	wildtype	Δ92-95 (*rpoD2*)
GCPH44	0.125	Type II non-mosaic (NG STAR 2.001)	421L	120G/121A	H553N	Δ92-95 (*rpoD2*)
GCGS0457 *rpoB1*	0.25	Type II non-mosaic (NG STAR 2.002)	421P	120G/121V	R201H (*rpoB1)*	wildtype
GCGS0457 *rpoD1*	0.25	Type II non-mosaic (NG STAR 2.002)	421P	120G/121V	wildtype	E98K (*rpoD1*)
GCGS0457 *rpoD2*	0.125	Type II non-mosaic (NG STAR 2.002)	421P	120G/121V	wildtype	Δ92-95 (*rpoD2*)
GCGS0364	0.023	Type II non-mosaic (NG STAR 2.002)	421P	120K/121D	wildtype	wildtype
GCGS0364 *rpoB2*	0.5	Type II non-mosaic (NG STAR 2.002)	421P	120K/121D	G158V (*rpoB2*)	wildtype
GCGS0364 *rpoB3*	0.75	Type II non-mosaic (NG STAR 2.002)	421P	120K/121D	P157L (*rpoB3*)	wildtype

Table 2. Antibiotic susceptibility profiles of CRO^{RS} strains with RNAP mutations.

Strain	MIC (μg/ml)							
	CRO	**CFX**	**PEN**	**EPM**	**AZI**	**TET**	**CIP**	**RIF**
GCGS0457	0.016	0.016	2	0.016	0.25	1	≤0.015	0.125
GCGS1095	0.5	1	2	0.032	0.5	1	≤0.015	≤0.0625
GCGS1014	0.125	0.5	1	0.032	0.25	1	≤0.015	≤0.0625
GCGS1013	0.125	0.5	0.5	0.023	0.5	1	≤0.015	≤0.0625
GCGS0457 RpoB^{R201H}	0.25	>0.5	1	0.047	0.25	1	≤0.015	≤0.0625
GCGS0457 RpoD^{E98K}	0.25	0.5	1	0.023	0.25	1	≤0.015	≤0.0625
GCGS0457 RpoD$^{Δ92-95}$	0.125	0.5	1	0.023	0.25	1	≤0.015	≤0.0625

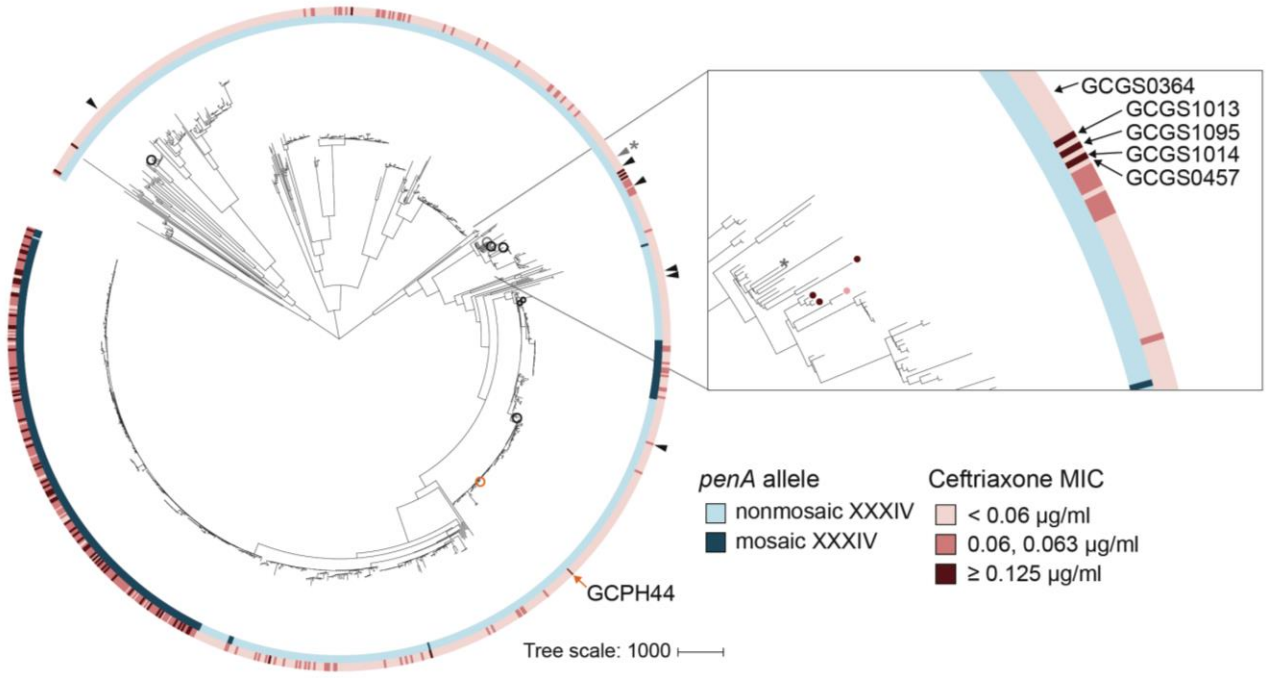

Figure 1. RNA polymerase-mediated reduced cephalosporin susceptibility among GISP isolates. Most high-level reduced cephalosporin susceptibility (MIC ≥ 0.125 µg/mL) in the GISP dataset is associated with the mosaic *penA* XXXIV allele, but some isolates with high MICs lack this allele (left). In four of these isolates – GCGS1095, GCGS1014, GCGS1013 (inset, red-marked leaves) and the U.K. isolate GCPH44 (left, orange circle) – CRO^{RS} is caused by mutations in the RNA polymerase holoenzyme. Transformation of the CRO^{RS} allele *rpoB1* from GCGS1095 confers phenotypic reduced susceptibility to other susceptible clinical isolates (arrows and black-circled leaves, left) such as the phylogenetic neighbor GCGS0457 (inset, pink-marked leaf). The isolate GCGS0364 (gray, denoted with *) spontaneously develops CRO^{RS} via *rpoB* mutation *in vitro*.

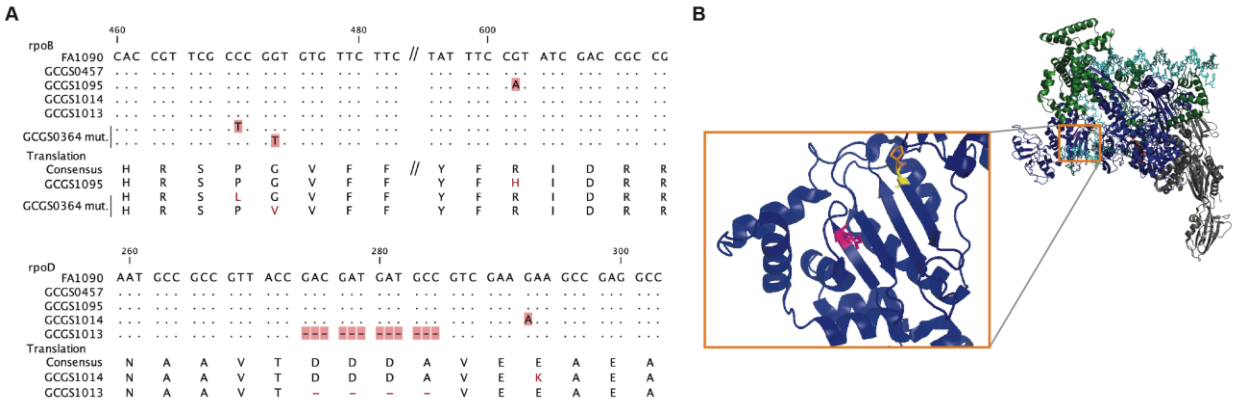

Figure 2. Location of CRO^{RS}-associated RNA polymerase mutations. (A) Alignment of mutant RNA polymerase alleles associated with reduced ceftriaxone susceptibility. **(B)** Crystal structure of the RNA polymerase holoenzyme from *E. coli* by Zuo *et al.* (PDB 4YLO) (Zuo & Steitz, 2015), showing the location of the residues homologous to *N. gonorrhoeae* RpoB R201 (magenta), G158 (yellow), and P157 (orange). The flexible region of σ^{70} 1.1 that includes the variant positions of *rpoD1* and *rpoD1* is not included in this structure, but is predicted to interact with this region of RpoB (Murakami, 2013).

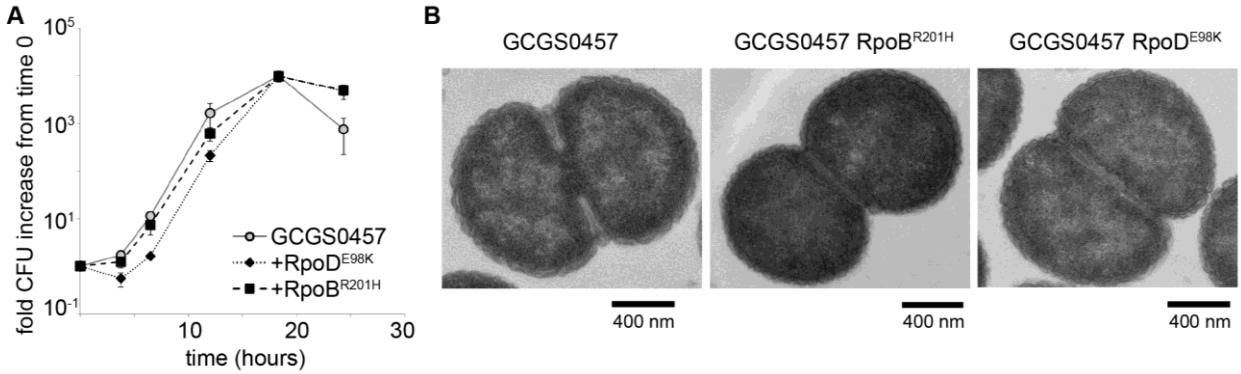

Figure 3. RNA polymerase mutations do not change growth phenotypes. (**A**) Growth of GCGS0457 and RNAP mutant transformants on solid GCB agar (n=3, representative of two independent experiments). RNAP mutations do not result in a growth rate defect. (**B**) Transmission electron micrographs of GCGS0457 and RNAP mutant transformants. CRO^{RS} transformants are slightly smaller than the parental GCGS0457 strain, but are otherwise morphologically similar.

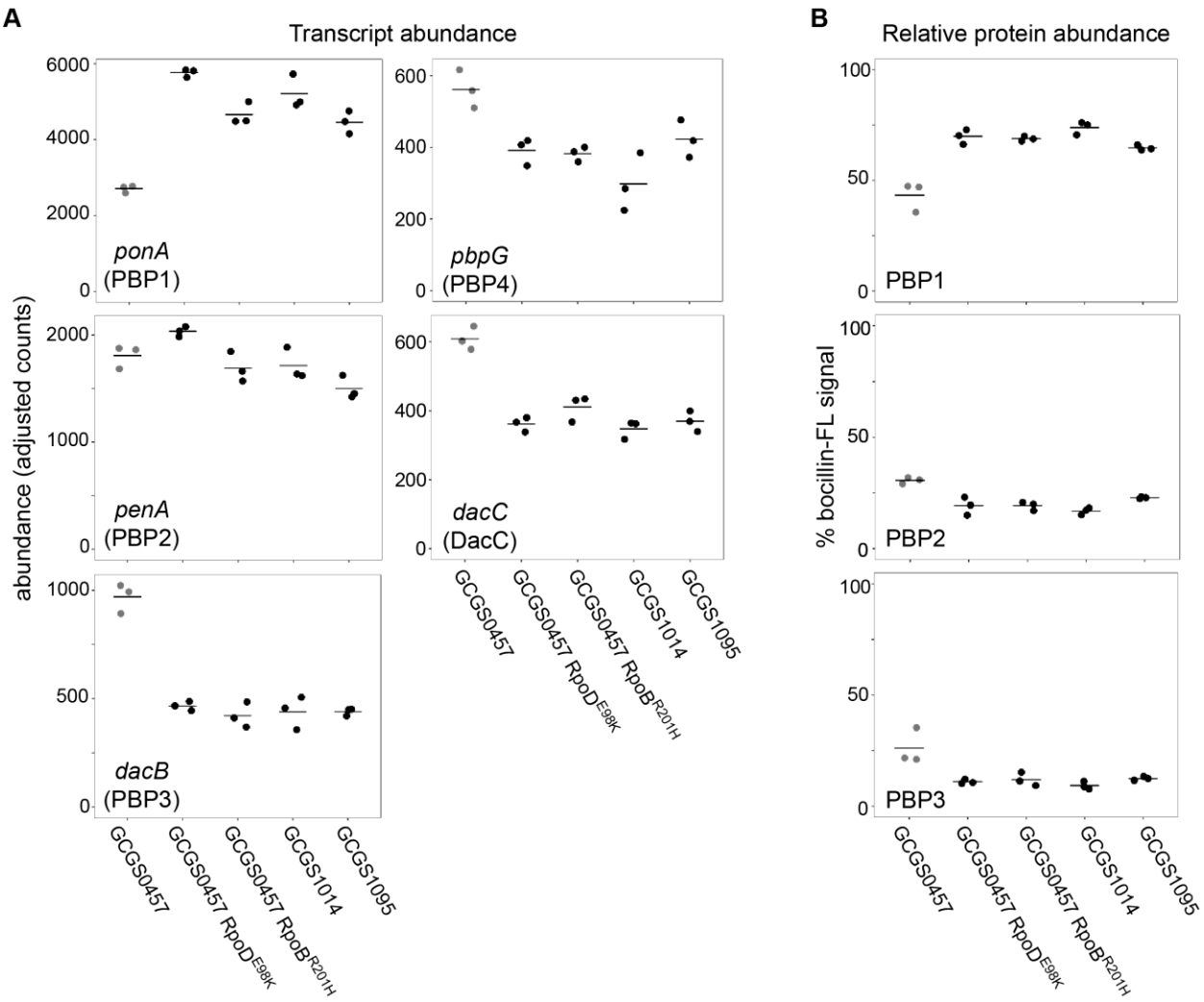

Figure 4. Effect of CRO^{RS}-associated RNA polymerase mutations on PBP abundance. (**A**) Normalized abundance of transcripts encoding penicillin binding proteins (PBPs) in parental isolates (GCGS0457, GCGS1095, GCGS1014) and RNAP mutant transformants in the GCGS0457 background, measured by RNAseq. (**B**) Relative protein abundance of PBP1, PBP2, and PBP3, as measured by bocillin-FL labeling. Total bocillin-FL signal for each strain was set at 100%. The relative contribution of each PBP to that signal is shown here. PBP4 protein was not observed on these gels, in agreement with previous reports (Zapun, Morlot, & Taha, 2016).

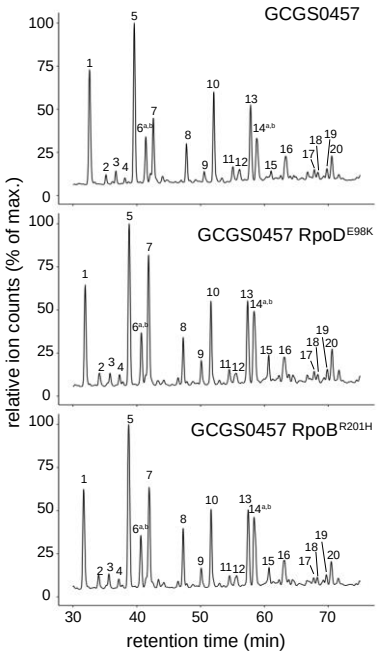

Peak	Proposed Structure	GCGS0457	GCGS0457 RpoD^{E98K}	GCGS0457 RpoB^{R201H}
1	Tripeptide	18.9	12.6	13.3
2	Tetrapeptide +Ala-mDAP	0.7	0.9	0.9
3	Peak 2 isomer	1.6	1.6	1.9
4	Pentapeptide (Gly)	0.4	0.9	0.8
5	Tetrapeptide	24.1	21.3	24.8
6a	Dipeptide	4.9	5.9	5.9
6b	Tripeptide (OAc)	2.8	1.9	2.1
7	Pentapeptide	8.1	15	12.2
8	Tetrapeptide (OAc)	4.3	4	5.4
9	Pentapeptide (OAc)	0.8	1.7	1.3
10	Tripeptide ($-H_2O$)	14.3	10.5	10.3
11	4-3 tetra-tri or 3-3 tri-tetra	0.8	0.6	0.4
12	Peak 11 isomer	0.6	0.5	0.5
13	4-3 tetra-tetra or 3-3 tri-penta	5.6	5	4.7
14a	Tetrapeptide ($-H_2O$)	4.6	6.7	7.8
14b	4-3 tetra-penta	1.6	2.6	1.9
15	Pentapeptide ($-H_2O$)	0.7	2.6	1.5
16	4-3 tetra-tetra or 3-3 tri-penta (OAc)	2	1.9	1.7
17	4-3 tetra-tri or 3-3 tri-tetra ($-H_2O$)	0.9	0.8	0.4
18	Peak 17 isomer	0.4	0.3	0.3
19	4-3 tetra-tetra or 3-3 tri-penta ($-H_2O$)	0.6	0.6	0.5
20	Peak 19 isomer	1.5	1.9	1.4
	Total Monomers	86.2	85.8	88.3
	Total Crosslinks	13.8	14.2	11.7

Figure 5. Effect of CRO^{RS}-associated RNA polymerase mutations on cell wall structure. Relative abundance of muropeptide peaks in cell wall digests of GCGS0457 and its CRO^{RS} derivatives, GCGS0457 RpoD^{E98K} and GCGS0457 RpoB^{R201H}. Transformant cell walls contain a higher proportion of peptidoglycan with pentapeptide stems (peaks 4, 7, 9, 14b, and 15). Data is representative of 3 independent experiments. Values were calculated by extracting the peak mass from the total ion chromatogram, integrating the resulting peak area, and dividing by the sum of all of the peak areas within each sample. See Supplementary Table 2 for a list of all muropeptide masses detected.

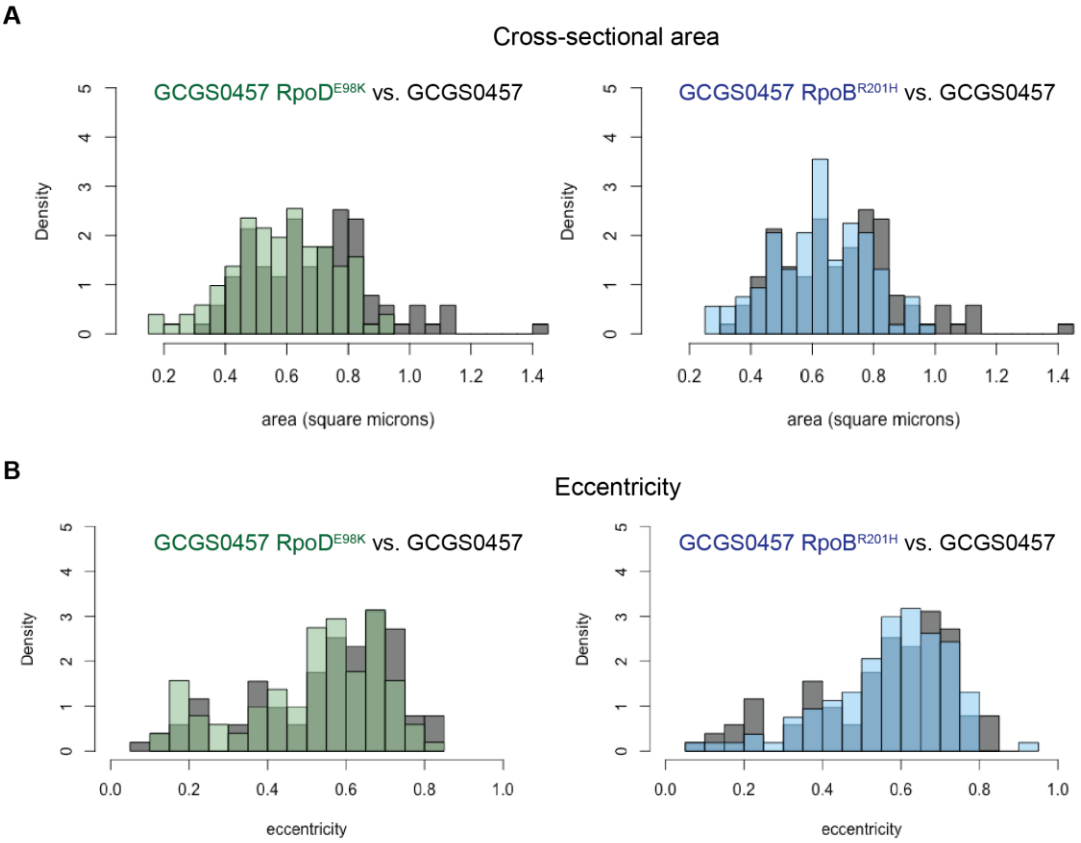

Supplementary Figure 1. Size and eccentricity of GCGS0457 and CRO^{RS} transformants. 100-105 cellular cross sections from TEM images were manually measured in ImageJ to measure the **(A)** cross-sectional area and **(B)** eccentricity of cells from the CRO^{S} strain GCGS0457 and its CRO^{RS} transformants GCGS0457 RpoD^{E98K} and GCGS0457 RpoB^{R201H}. The cross-sectional area of CRO^{RS} transformant cells is slightly smaller (mean area: 0.585 μm^2 for GCGS0457 RpoD^{E98K}; 0.621 μm^2 for GCGS0457 RpoB^{R201H}) than cells of the parental strain GCGS0457 (mean area 0.693 μm^2; $p = 3.977 \times 10^{-5}$ compared to GCGS0457 RpoD^{E98K} and p=0.00436 compared to GCGS0457 RpoB^{R201H} by Welch's t-test). The degree of eccentricity in the CRO cells is not significantly different between these populations.

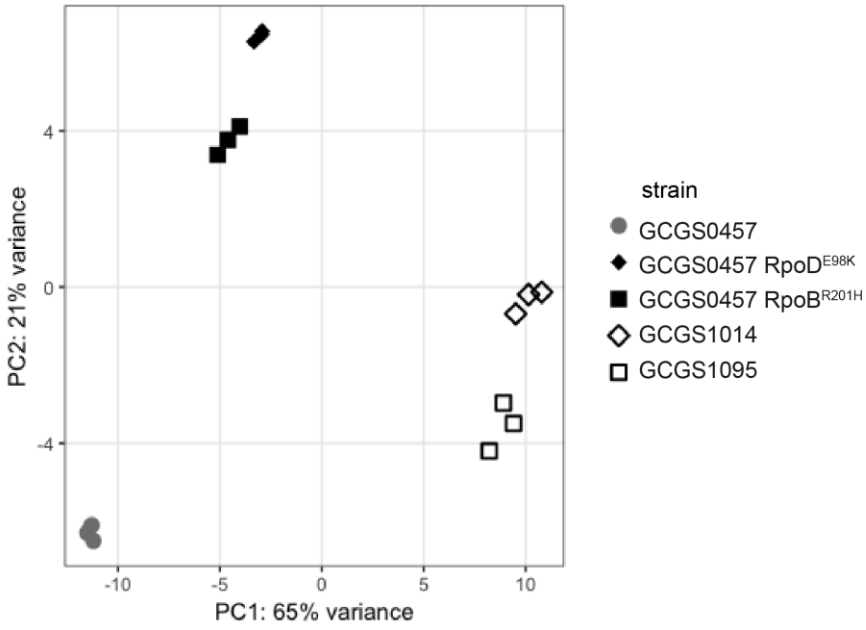

Supplementary Figure 2. Principle components analysis of RNA-seq data. The first two principle components are shown for transcriptomic data collected from the CRO^{S} isolate GCGS0457, the CRO^{RS} isolates GCGS1095 and GCGS1014, and the CRO^{RS} transformants GCGS0457 $RpoD^{E98K}$ and GCGS0457 $RpoB^{R201H}$ (three biological replicates/strain). Replicates from both CRO^{RS} transformants cluster tightly, despite having different RNAP mutations.

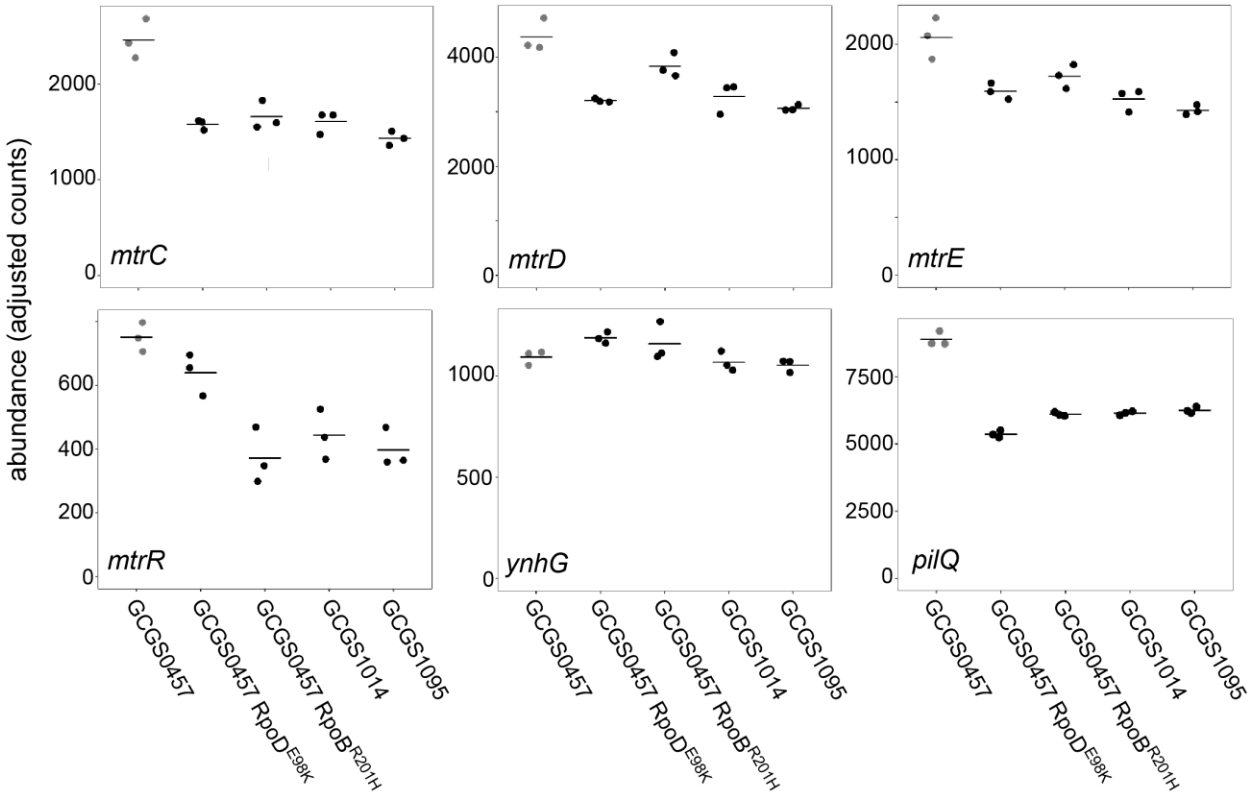

Supplementary Figure 3. Transcript abundance of various genes in CRO^{RS} strains with RNA polymerase mutations. Normalized abundance of various transcripts in parental isolates (GCGS0457, GCGS1095, GCGS1014) and RNAP mutant transformants in the GCGS0457 background. Shown: *mtrC*, *mtrD*, and *mtrE*, which encode the components of the Mtr efflux pump; *mtrR*, which encodes the transcriptional repressor of the *mtrCDE* operon; *ynhG*, a putative L,D-transpeptidase; and *pilQ*, which encodes the pilus pore subunit PilQ.

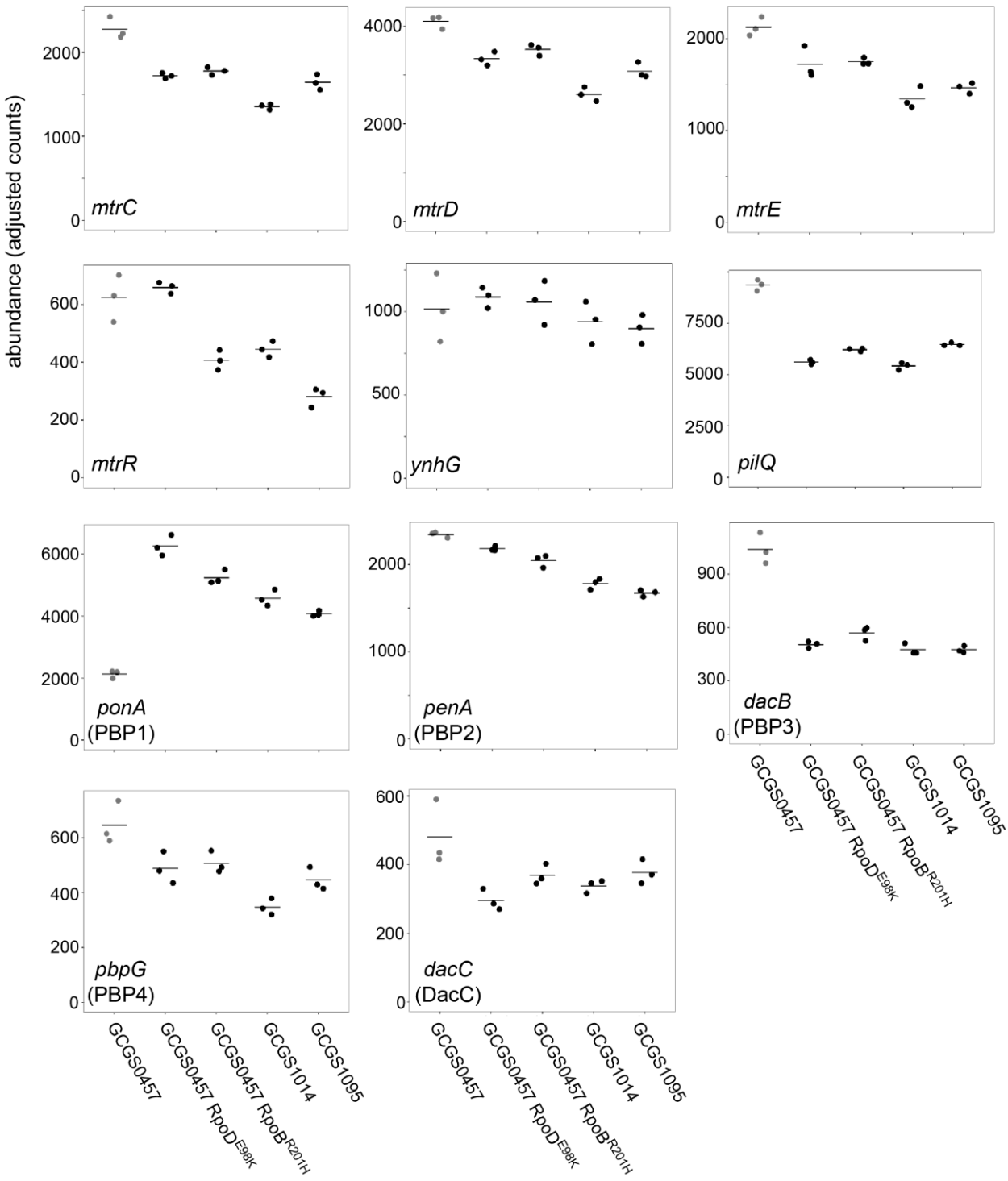

Supplementary Figure 4. Transcript abundance of various genes in CRO^{RS} strains with RNAP mutations, exposed to sub-inhibitory ceftriaxone. Normalized abundance of various transcripts in parental isolates (GCGS0457, GCGS1095, GCGS1014) and RNAP mutant transformants, exposed to 0.008 µg/mL CRO for 90 minutes. Shown: *mtrC*, *mtrD*, and *mtrE*, which encode the components of the Mtr efflux pump; *mtrR*, which encodes the transcriptional

repressor of the *mtrCDE* operon; *ynhG*, a putative L,D-transpeptidase; *pilQ*, which encodes the pilus pore subunit PilQ; and transcripts for each of the penicillin-binding proteins.

Supplementary Table 1. *N. gonorrhoeae* strains used in this study

Strain name	Description	Source	Strain number
GCGS0457	CRO^{S} clinical isolate; recipient strain for transformations	GISP, CDC	
GCGS1013	CRO^{RS} clinical isolate	GISP, CDC	
GCGS1014	CRO^{RS} clinical isolate	GISP, CDC	
GCGS1095	CRO^{RS} clinical isolate	GISP, CDC	
GCPH44	CRO^{RS} clinical isolate	(De Silva et al., 2016)	
28BL	CRO^{S} laboratory strain	Gift of S. Johnson	
FA1090	CRO^{S} laboratory strain	Gift of C. Genco	
SP300-SP311	12 independent CRO^{RS} transformants: GCGS0457 + gDNA from GCGS1014	This study	
SP312-SP314	3 independent CRO^{RS} transformants: GCGS0457 + gDNA from GCGS1095	This study	
GCGS0457 RpoD^{E98K}	Point mutation introduced on PCR product	This study	SP316
GCGS0457 RpoB^{R201H}	Point mutation introduced on PCR product	This study	SP319
GCGS0457 RpoD$^{\Delta 92\text{-}95}$	Deletion introduced on PCR product	This study	SP323
GCGS0092	CRO^{S} clinical isolate	GISP, CDC	
GCGS0092 RpoB^{R201H}	CRO^{RS} transformant; point mutation introduced on PCR product	This study	SP349
GCGS0275	CRO^{S} clinical isolate	GISP, CDC	
GCGS0275 RpoB^{R201H}	CRO^{RS} transformant; point mutation introduced on PCR product	This study	SP354
GCGS0465	CRO^{S} clinical isolate	GISP, CDC	
GCGS0465 RpoB^{R201H}	CRO^{RS} transformant; point mutation introduced on PCR product	This study	SP358
GCGS0336	CRO^{S} clinical isolate	GISP, CDC	
GCGS0336 RpoB^{R201H}	CRO^{RS} transformant; point mutation introduced on PCR product	This study	SP340
GCGS0524	CRO^{S} clinical isolate	GISP, CDC	
GCGS0524 RpoB^{R201H}	CRO^{RS} transformant; point mutation introduced on PCR product	This study	SP368
GCGS0364	CRO^{S} clinical isolate; develops spontaneous CRO^{RS} via *rpoB* mutation *in vitro*	GISP, CDC	
GCGS0364 RpoB^{G158V}	Point mutation introduced on PCR product	This study	SP377
GCGS0364 RpoB^{P157L}	Point mutation introduced on PCR product	This study	SP375

Supplementary Table 2. Muropeptide masses detected in cell wall digests of GCGS0457 and RNAP mutants.

Peak	Proposed Structure[a]	Theoretical Mass (charge)	Observed Mass (charge)
1	Tripeptide	871.3779 (1), 436.1926 (2)	871.3783 (1), 436.1925 (2)
2	Tetrapeptide +Ala-mDAP[2]	1185.5369 (1), 593.2721 (2)	593.2719 (2)
3	Peak 2 isomer	1185.5369 (1), 593.2721 (2)	593.2721 (2)
4	Pentapeptide (Gly)	999.4364 (1), 500.2219 (2)	999.4360 (1), 500.2213 (2)
5	Tetrapeptide	942.4150 (1), 471.7111 (2)	942.4151 (1), 471.7109 (2)
6a	Dipeptide	699.2931 (1), 721.275 (1+Na)	699.2937 (1), 721.2754 (1+Na)
6b	Tripeptide (OAc)	913.3884 (1), 457.1979 (2)	913.3893 (1), 457.1974
7	Pentapeptide	1013.4521 (1), 507.2297 (2)	1013.4527 (1), 507.2297 (2)
8	Tetrapeptide (OAc)	984.4255 (1), 492.7164 (2)	984.4264 (1), 492.7163 (2)
9	Pentapeptide (OAc)	1055.4627 (1), 528.235 (2)	1055.4684 (1), 528.2345 (2)
10	Tripeptide ($-H_2O$)	851.3517 (1), 426.1795 (2)	851.3520 (1)
11	4-3 tetra-tri or 3-3 tri-tetra[c]	897.8911 (2), 598.9299 (3)	897.8924 (2), 598.9295 (3)
12	Peak 11 isomer	897.8911 (2), 598.9299 (3)	897.8924 (2), 598.9295 (3)
13	4-3 tetra-tetra or 3-3 tri-penta[c]	933.4097 (2), 622.6089 (3)	933.4117 (2), 622.6091 (3)
14a	Tetrapeptide ($-H_2O$)	922.3888 (1), 461.698 (2)	922.3906 (1), 461.6981 (2)
14b	4-3 tetra-penta	968.9283 (2), 646.2879 (3)	968.9309 (2), 646.2888 (3)
15	Pentapeptide ($-H_2O$)	993.4259 (1), 497.2166 (2)	933.4257 (1), 497.2163 (2)
16	4-3 tetra-tetra or 3-3 tri-penta (OAc)[c]	954.4150 (2), 636.6124 (3)	954.4165 (2), 636.6124 (2)
17	4-3 tetra-tri or 3-3 tri-tetra ($-H_2O$)[c]	887.878 (2), 592.2544 (3)	887.8792 (2), 592.2543 (3)
18	Peak 17 isomer	887.878 (2), 592.2544 (3)	887.8792 (2), 592.2543 (3)
19	4-3 tetra-tetra or 3-3 tri-penta ($-H_2O$)[c]	923.3966 (2), 615.9335 (3)	923.3977 (2), 615.9332 (3)
20	Peak 19 isomer	923.3966 (2), 615.9335 (3)	923.3977 (2), 615.9332 (3)

[a] The pentapeptide stem in *N. gonorrhoeae* is L-Ala-γ-D-Glu-L-mDap-D-Ala-D-Ala. OAc = O-acetylation of MurNAc. $-H_2O$ = 1,6-anhdro-MurNAc. Gly = replacement of one D-Ala residue with glycine.

[b] This structure is the product of cleavage of a 4-3 crosslink.

[c] Mass is consistent with either a 4-3 (PBP-mediated) crosslink or a 3-3 (L,D-transpeptidase-mediated) crosslink.

Supplementary File 1 (Excel workbook). Allelic diversity of RNA polymerase holoenzyme components and sigma factors.

References

Abrams, A. Jeanine, Kirkcaldy, Robert D., Pettus, Kevin, Fox, Jan L., Kubin, Grace, & Trees, David L. (2017). A Case of Decreased Susceptibility to Ceftriaxone in Neisseria gonorrhoeae in the Absence of a Mosaic Penicillin-Binding Protein 2 (penA) Allele. *Sexually Transmitted Diseases, 44*, 492-494. doi: 10.1097/OLQ.0000000000000645

Allan-Blitz, L. T., Humphries, R. M., Hemarajata, P., Bhatti, A., Pandori, M. W., Siedner, M. J., & Klausner, J. D. (2017). Implementation of a Rapid Genotypic Assay to Promote Targeted Ciprofloxacin Therapy of Neisseria gonorrhoeae in a Large Health System. *Clin Infect Dis, 64*(9), 1268-1270. doi: 10.1093/cid/ciw864

Ambur, O. Herman, Frye, Stephan A., & Tønjum, Tone. (2007). New functional identity for the DNA uptake sequence in transformation and its presence in transcriptional terminators. *J Bacteriol, 189*, 2077-2085. doi: 10.1128/JB.01408-06

Atkinson, B. L., & Gottesman, M. E. (1992). The Escherichia coli rpoB60 mutation blocks antitermination by coliphage HK022 Q-function. *J Mol Biol, 227*(1), 29-37. doi: 10.1016/0022-2836(92)90679-e

Bankevich, A., Nurk, S., Antipov, D., Gurevich, A. A., Dvorkin, M., Kulikov, A. S., . . . Pevzner, P. A. (2012). SPAdes: a new genome assembly algorithm and its applications to single-cell sequencing. *J Comput Biol, 19*(5), 455-477. doi: 10.1089/cmb.2012.0021

Centers for Disease Control and Prevention. (2018, July 24, 2018). Gonorrhea -- Sexually Transmitted Disease Surveillance 2017. Retrieved March 22, 2019, from https://http://www.cdc.gov/std/stats17/gonorrhea.htm

Chen, C. J., Tobiason, D. M., Thomas, C. E., Shafer, W. M., Seifert, H. S., & Sparling, P. F. (2004). A mutant form of the Neisseria gonorrhoeae pilus secretin protein PilQ allows increased entry of heme and antimicrobial compounds. *J Bacteriol, 186*(3), 730-739. doi: 10.1128/jb.186.3.730-739.2004

Crofts, Terence S., Gasparrini, Andrew J., & Dantas, Gautam. (2017). Next-generation approaches to understand and combat the antibiotic resistome. *Nature Reviews Microbiology, 15*, 422-434. doi: 10.1038/nrmicro.2017.28

Croucher, N. J., Page, A. J., Connor, T. R., Delaney, A. J., Keane, J. A., Bentley, S. D., . . . Harris, S. R. (2015). Rapid phylogenetic analysis of large samples of recombinant bacterial whole genome sequences using Gubbins. *Nucleic Acids Res, 43*(3), e15. doi: 10.1093/nar/gku1196

Cui, Longzhu, Isii, Taisuke, Fukuda, Minoru, Ochiai, Tomonori, Neoh, Hui Min, Da Cunha Camargo, Ilana Lopes Baratella, . . . Hiramatsu, Keiichi. (2010). An RpoB mutation confers dual heteroresistance to daptomycin and vancomycin in Staphylococcus aureus. *Antimicrob Agents Chemother, 54*, 5222-5233. doi: 10.1128/AAC.00437-10

De Silva, D., Peters, J., Cole, K., Cole, M. J., Cresswell, F., Dean, G., . . . Eyre, D. W. (2016). Whole-genome sequencing to determine transmission of Neisseria gonorrhoeae: an observational study. *Lancet Infect Dis, 16*(11), 1295-1303. doi: 10.1016/S1473-3099(16)30157-8

Demczuk, Walter, Lynch, Tarah, Martin, Irene, Van Domselaar, Gary, Graham, Morag, Bharat, Amrita, . . . Mulvey, Michael R. (2015). Whole-genome phylogenomic heterogeneity of Neisseria gonorrhoeae isolates with decreased cephalosporin susceptibility collected in Canada between 1989 and 2013. *Journal of Clinical Microbiology, 53*, 191-200. doi: 10.1128/JCM.02589-14

Deng, X., Allan-Blitz, L. T., & Klausner, J. D. (2019). Using the genetic characteristics of Neisseria gonorrhoeae strains with decreased susceptibility to cefixime to develop a molecular assay to predict cefixime susceptibility. *Sex Health*. doi: 10.1071/SH18227

Eyre, David W, Sanderson, Nicholas D, Lord, Emily, Regisford-Reimmer, Natasha, Chau, Kevin, Barker, Leanne, . . . Andersson, Monique I. (2018). Gonorrhoea treatment failure caused by a Neisseria gonorrhoeae strain with combined ceftriaxone and high- level azithromycin resistance, England, February 2018. *Eurosurveillance, 23*, 1800323. doi: 10.2807/1560-7917.ES.2018.23.27.1800323

Eyre, David W, Town, Katy, Street, Teresa, Barker, Leanne, Sanderson, Nicholas, Cole, Michelle J, . . . Fifer, Helen. (2019). Detection in the United Kingdom of the Neisseria gonorrhoeae FC428 clone, with ceftriaxone resistance and intermediate resistance to azithromycin, October to December 2018. *Eurosurveillance, 24*. doi: 10.2807/1560-7917.ES.2019.24.10.1900147

Eyre, David W., De Silva, Dilrini, Cole, Kevin, Peters, Joanna, Cole, Michelle J., Grad, Yonatan H., . . . Paul, John. (2017). WGS to predict antibiotic MICs for Neisseria gonorrhoeae. *Journal of Antimicrobial Chemotherapy*. doi: 10.1093/jac/dkx067

Fifer, Helen, Saunders, John, Soni, Suneeta, Sadiq, Syed Tariq, & FitzGerald, Mark. (2019). British Association for Sexual Health and HIV national guideline for the management of infection with Neisseria gonorrhoeae (2019). 1-25.

Grad, Yonatan H, Harris, Simon R, Kirkcaldy, Robert D, Green, Anna G, Marks, Debora S, Bentley, Stephen D, . . . Lipsitch, Marc. (2016). Genomic epidemiology of gonococcal resistance to extended-spectrum cephalosporins, macrolides, and fluoroquinolones in the United States, 2000-2013. *J Infect Dis, 214*, 1579-1587. doi: 10.1093/infdis/jiw420

Guérillot, Romain, Gonçalves da Silva, Anders, Monk, Ian, Giulieri, Stefano, Tomita, Takehiro, Alison, Eloise, . . . Howden, Benjamin P. (2018). Convergent Evolution Driven by Rifampin Exacerbates the Global Burden of Drug-Resistant Staphylococcus aureus. *mSphere, 3*, 1-15.

Hicks, Allison L., Kissler, Stephen M., Lipsitch, Marc, & Grad, Yonatan H. (2019). Quantifying the surveillance required to sustain genetic marker-based antibiotic resistance diagnostics. *bioRxiv*, 699918. doi: 10.1101/699918

Johnson, Steven R., Grad, Yonatan, Ganakammal, Satishkumar Ranganathan, Burroughs, Mark, Frace, Mike, Lipsitch, Marc, . . . Trees, David. (2014). In vitro selection of Neisseria gonorrhoeae mutants with elevated MIC values and increased resistance to cephalosporins. *Antimicrob Agents Chemother, 58*, 6986-6989. doi: 10.1128/AAC.03082-14

Kellogg, Douglas S., Peacock, William L., Deacon, W. E., Brown, L., & Pirkle, Carl I. (1963). Neisseria gonorrhoeae: Virulence genetically linked to clonal variation. *J Bacteriol, 85*, 1274-1279.

Kim, S., De Jonghe, J., Kulesa, A. B., Feldman, D., Vatanen, T., Bhattacharyya, R. P., . . . Blainey, P. C. (2017). High-throughput automated microfluidic sample preparation for accurate microbial genomics. *Nat Commun, 8*, 13919. doi: 10.1038/ncomms13919

Kirkcaldy, Robert D., Harvey, Alesia, Papp, John R., del Rio, Carlos, Soge, Olusegun O., Holmes, King K., . . . Torrone, Elizabeth. (2016). Neisseria gonorrhoeae Antimicrobial Susceptibility Surveillance — The Gonococcal Isolate Surveillance Project, 27 Sites, United States, 2014. *MMWR. Surveillance Summaries, 65*, 1-19. doi: 10.15585/mmwr.ss6507a1

Kocaoglu, Ozden, & Carlson, Erin E. (2015). Profiling of β-lactam selectivity for penicillin-binding proteins in Escherichia coli strain DC2. *Antimicrob Agents Chemother, 59*, 2785-2790. doi: 10.1128/AAC.04552-14

Kristich, Christopher J., & Little, Jaime L. (2012). Mutations in the beta subunit of RNA polymerase alter intrinsic cephalosporin resistance in enterococci. *Antimicrob Agents Chemother, 56*, 2022-2027. doi: 10.1128/AAC.06077-11

Kühner, Daniel, Stahl, Mark, Demircioglu, Dogan D., & Bertsche, Ute. (2014). From cells to muropeptide structures in 24 h: Peptidoglycan mapping by UPLC-MS. *Sci Rep, 4*, 7494. doi: 10.1038/srep07494

Lee, Jean Y. H., Monk, Ian R., Gonçalves da Silva, Anders, Seemann, Torsten, Chua, Kyra Y. L., Kearns, Angela, . . . Howden, Benjamin P. (2018). Global spread of three multidrug-resistant lineages of Staphylococcus epidermidis. *Nature Microbiology*. doi: 10.1038/s41564-018-0230-7

Lee, Yong Heon, Nam, Ki Hyun, & Helmann, John D. (2013). A mutation of the RNA polymerase beta prime subunit (rpoC) confers cephalosporin resistance in Bacillus subtilis. *Antimicrob Agents Chemother, 57*, 56-65. doi: 10.1128/AAC.01449-12

Letunic, I., & Bork, P. (2019). Interactive Tree Of Life (iTOL) v4: recent updates and new developments. *Nucleic Acids Res, 47*(W1), W256-W259. doi: 10.1093/nar/gkz239

Li, Heng. (2013). Aligning sequence reads, clone sequences and assembly contigs with BWA-MEM. *arXiv*, 13033997.

Li, Heng, & Durbin, Richard. (2010). Fast and accurate long-read alignment with Burrows-Wheeler transform. *Bioinformatics, 26*, 589-595. doi: 10.1093/bioinformatics/btp698

Lindberg, Robert, Fredlund, Hans, Nicholas, Robert, & Unemo, Magnus. (2007). Neisseria gonorrhoeae isolates with reduced susceptibility to cefixime and ceftriaxone: Association with genetic polymorphisms in penA, mtrR, porB1b, and ponA. *Antimicrob Agents Chemother, 51*, 2117-2122. doi: 10.1128/AAC.01604-06

Love, Michael I., Huber, Wolfgang, & Anders, Simon. (2014). Moderated estimation of fold change and dispersion for RNA-seq data with DESeq2. *Genome Biology, 15*, 1-21. doi: 10.1186/s13059-014-0550-8

Morse, S. A., Johnson, S. R., Biddle, J. W., & Roberts, M. C. (1986). High-level tetracycline resistance in Neisseria gonorrhoeae is result of acquisition of streptococcal tetM determinant. *Antimicrob Agents Chemother, 30*, 664-670. doi: 10.1128/AAC.30.5.664

Murakami, K. S. (2013). X-ray crystal structure of Escherichia coli RNA polymerase sigma70 holoenzyme. *J Biol Chem, 288*(13), 9126-9134. doi: 10.1074/jbc.M112.430900

Nandi, Sobhan, Swanson, Shauna, Tomberg, Joshua, & Nicholas, Robert A. (2015). Diffusion of antibiotics through the PilQ secretin in Neisseria gonorrhoeae occurs through the immature, sodium dodecyl sulfate-labile form. *J Bacteriol, 197*, 1308-1321. doi: 10.1128/JB.02628-14

Obergfell, Kyle P., Schaub, Ryan E., Priniski, Lauren L., Dillard, Joseph P., & Seifert, H. Steven. (2018). The low-molecular-mass, penicillin-binding proteins DacB and DacC combine to modify peptidoglycan cross-linking and allow stable Type IV pilus expression in Neisseria gonorrhoeae. *Molecular Microbiology, 109*, 135-149. doi: 10.1111/mmi.13955

Obuchowski, M., Giladi, H., Koby, S., Szalewska-Palasz, A., Wegrzyn, A., Oppenheim, A. B., . . . Wegrzyn, G. (1997). Impaired lysogenisation of the Escherichia coli rpoA341 mutant by

bacteriophage lambda is due to the inability of CII to act as a transcriptional activator. *Mol Gen Genet, 254*(3), 304-311.

Peng, Jun-Ping, Yin, Yue-Ping, Chen, Shao-Chun, Yang, Jian, Dai, Xiu-Qin, Zheng, He-Ping, . . . Jin, Qi. (2019). A Whole-genome Sequencing Analysis of Neisseria gonorrhoeae Isolates in China: An Observational Study. *EClinicalMedicine, 7*, 47-54. doi: 10.1016/j.eclinm.2019.01.010

Penwell, William F., Shapiro, Adam B., Giacobbe, Robert A., Gu, Rong Fang, Gao, Ning, Thresher, Jason, . . . Miller, Alita A. (2015). Molecular mechanisms of sulbactam antibacterial activity and resistance determinants in Acinetobacter baumannii. *Antimicrob Agents Chemother, 59*, 1680-1689. doi: 10.1128/AAC.04808-14

Public Health England. (2018). Surveillance of antimicrobial resistance in Neisseria gonorrhoeae in England and Wales. Key findings from the Gonococcal Resistance to Antimicrobials Surveillance Programme (GRASP). Anti-microbial resistance in Neisseria gonorrhoeae: data to May 2018 (pp. 1-25). London, United Kingdom: Public Health England.

Rudel, Thomas, van Putten, Jos P.M., Gibbs, Carol P., Haas, Rainer, & Meyer, Thomas F. (1992). Interaction of two variable proteins (PilE and PilC) required for pilus-mediated adherence of Neisseria gonorrhoeae to human epithelial cells. *Molecular Microbiology, 6*, 3439-3450. doi: 10.1111/j.1365-2958.1992.tb02211.x

Rudy, Robert F, Patel, Milesh M, Busby, Michele, Bhattacharyya, Roby P, Shishkin, Alexander A, Chen, Jenny, . . . Guttman, Mitchell. (2015). Simultaneous generation of many RNA-seq libraries in a single reaction. *Nature Methods, 12*, 323-325. doi: 10.1038/nmeth.3313

Sauvage, Eric, Kerff, Frédéric, Terrak, Mohammed, Ayala, Juan A., & Charlier, Paulette. (2008). The penicillin-binding proteins: Structure and role in peptidoglycan biosynthesis. *FEMS Microbiology Reviews, 32*, 234-258. doi: 10.1111/j.1574-6976.2008.00105.x

Schneider, Caroline A, Rasband, Wayne S, & Eliceiri, Kevin W. (2012). NIH Image to ImageJ: 25 years of image analysis. *Nature Methods, 9*, 671-675. doi: 10.1038/nmeth.2089

Stamatakis, A. (2014). RAxML version 8: a tool for phylogenetic analysis and post-analysis of large phylogenies. *Bioinformatics, 30*(9), 1312-1313. doi: 10.1093/bioinformatics/btu033

Tuite, Ashleigh R, Gift, Thomas L, Chesson, Harrell W, Hsu, Katherine, Salomon, Joshua A, & Grad, Yonatan H. (2017). Impact of Rapid Susceptibility Testing and Antibiotic Selection Strategy on the Emergence and Spread of Antibiotic Resistance in Gonorrhea. *The Journal of Infectious Diseases, 216*, 1-22. doi: 10.1093/infdis/jix450

Wadsworth, C. B., Sater, M. R. A., Bhattacharyya, R. P., & Grad, Y. H. (2019). Impact of species diversity on the design of RNA-based diagnostics for antibiotic resistance in Neisseria gonorrhoeae. *Antimicrob Agents Chemother*. doi: 10.1128/AAC.00549-19

Wadsworth, Crista B, Arnold, Brian J, Abdul Sater, Mohamad R, & Grad, Yonatan H. (2018). Azithromycin Resistance through Interspecific Acquisition of an Epistasis-Dependent Efflux Pump Component and Transcriptional Regulator in Neisseria gonorrhoeae. *mBio, 9*, e01419-01418.

Walker, Bruce J., Abeel, Thomas, Shea, Terrance, Priest, Margaret, Abouelliel, Amr, Sakthikumar, Sharadha, . . . Earl, Ashlee M. (2014). Pilon: An integrated tool for comprehensive microbial variant detection and genome assembly improvement. *PLoS ONE, 9*. doi: 10.1371/journal.pone.0112963

Wang, Yubing, Li, Xiaoli, Jiang, Libo, Han, Wentao, Xie, Xiangming, Jin, Yi, . . . Wu, Rongling. (2017). Novel Mutation Sites in the Development of Vancomycin-

Intermediate Resistance in Staphylococcus aureus. *Frontiers in Microbiology, 7*, 1-12. doi: 10.3389/fmicb.2016.02163

Watanabe, Yukiko, Cui, Longzhu, Katayama, Yuki, Kozue, Kishii, & Hiramatsu, Keiichi. (2011). Impact of rpoB mutations on reduced vancomycin susceptibility in Staphylococcus aureus. *Journal of Clinical Microbiology, 49*, 2680-2684. doi: 10.1128/JCM.02144-10

Whiley, D. M., Limnios, E. A., Ray, S., Sloots, T. P., & Tapsall, J. W. (2007). Diversity of penA alterations and subtypes in Neisseria gonorrhoeae strains from Sydney, Australia, that are less susceptible to ceftriaxone. *Antimicrob Agents Chemother*, *51*(9), 3111-3116. doi: 10.1128/AAC.00306-07

Whiley, David M., Goire, Namraj, Lambert, Stephen B., Ray, Sanghamitra, Limnios, E. Athena, Nissen, Michael D., . . . Tapsall, John W. (2010). Reduced susceptibility to ceftriaxone in Neisseria gonorrhoeae is associated with mutations G542S, P551S and P551L in the gonococcal penicillin-binding protein 2. *Journal of Antimicrobial Chemotherapy, 65*, 1615-1618. doi: 10.1093/jac/dkq187

Zapun, André, Morlot, Cécile, & Taha, Muhamed-Kheir. (2016). Resistance to β-Lactams in Neisseria ssp Due to Chromosomally Encoded Penicillin-Binding Proteins. *Antibiotics, 5*, 35. doi: 10.3390/antibiotics5040035

Zerbino, D. R., & Birney, E. (2008). Velvet: algorithms for de novo short read assembly using de Bruijn graphs. *Genome Res, 18*(5), 821-829. doi: 10.1101/gr.074492.107

Zhao, L., Liu, A., Li, R., & Zhao, S. (2019). Multiplex TaqMan real-time PCR platform for detection of Neisseria gonorrhoeae with decreased susceptibility to ceftriaxone. *Diagn Microbiol Infect Dis, 93*(4), 299-304. doi: 10.1016/j.diagmicrobio.2018.10.013

Zhao, Shuqing, Duncan, Margaret, Tomberg, Joshua, Davies, Christopher, Unemo, Magnus, & Nicholas, Robert A. (2009). Genetics of chromosomally mediated intermediate resistance to ceftriaxone and cefixime in Neisseria gonorrhoeae. *Antimicrob Agents Chemother, 53*, 3744-3751. doi: 10.1128/AAC.00304-09

Zhao, Shuqing, Tobiason, Deborah M., Hu, Mei, Seifert, H. Steven, & Nicholas, Robert A. (2005). The penC mutation conferring antibiotic resistance in Neisseria gonorrhoeae arises from a mutation in the PilQ secretin that interferes with multimer stability. *Molecular Microbiology, 57*, 1238-1251. doi: 10.1111/j.1365-2958.2005.04752.x

Zhu, Y. Y., Machleder, E. M., Chenchik, A., Li, R., & Siebert, P. D. (2001). Reverse transcriptase template switching: A SMART™ approach for full-length cDNA library construction. *BioTechniques, 30*, 892-897. doi: 10.2144/01304pf02

Zuo, Yuhong, & Steitz, Thomas A. (2015). Crystal structures of the E. coli transcription initiation complexes with a complete bubble. *Molecular Cell, 58*, 534-540. doi: 10.1016/j.molcel.2015.03.010